

Restoration by Compression

Yehuda Dar, Michael Elad, and Alfred M. Bruckstein

Abstract—In this paper we study the topic of signal restoration using complexity regularization, quantifying the compression bit-cost of the signal estimate. While complexity-regularized restoration is an established concept, solid practical methods were suggested only for the Gaussian denoising task, leaving more complicated restoration problems without a generally constructive approach. Here we present practical methods for complexity-regularized restoration of signals, accommodating deteriorations caused by a known linear degradation operator of an arbitrary form. Our iterative procedure, obtained using the Half Quadratic Splitting approach, addresses the restoration task as a sequence of simpler problems involving ℓ_2 -regularized estimations and rate-distortion optimizations (considering the squared-error criterion). Further, we replace the rate-distortion optimizations with an arbitrary standardized compression technique and thereby restore the signal by leveraging underlying models designed for compression. Additionally, we propose a shift-invariant complexity regularizer, measuring the bit-cost of all the shifted forms of the estimate, extending our method to use averaging of decompressed outputs gathered from compression of shifted signals. On the theoretical side, we present an analysis of complexity-regularized restoration of a cyclo-stationary Gaussian signal from deterioration by a linear shift-invariant operator and an additive white Gaussian noise. The theory shows that optimal complexity-regularized restoration relies on an elementary restoration filter and compression spreading reconstruction quality unevenly based on the energy distribution of the degradation filter. Nicely, these ideas are realized also in the proposed practical methods. Finally, we present experiments showing good results for image deblurring and inpainting using the HEVC compression standard.

Index Terms—Complexity regularization, rate-distortion optimization, signal restoration, image deblurring, half quadratic splitting.

I. INTRODUCTION

Signal restoration methods are often posed as inverse problems using regularization terms. While many solutions can explain a given degraded signal, using regularization will provide signal estimates based on prior assumptions on signals. One interesting regularization type measures the complexity of the candidate solution in terms of its compression bit-cost. Indeed, encoders (that yield the bit cost) rely on signal models and allocate shorter representations to more likely signal instances. This approach of complexity-regularized restoration is an attractive meeting point of signal restoration and compression, two fundamental signal-processing problems.

Numerous works [1]–[3] considered the task of denoising a signal corrupted by an additive white Gaussian noise using complexity regularization, practically estimating the clean signal by employing a standard lossy compression of its noisy version. However, more complex restoration problems (e.g.,

deblurring, super resolution, inpainting), involving non-trivial degradation operators, do not lend themselves to a straightforward treatment by compression techniques designed for the squared-error distortion measure. Moulin and Liu [4] studied the complexity regularization idea for general restoration problems, presenting a thorough theoretical treatment together with a limited practical demonstration of Poisson denoising based on a suitably designed compression method. Indeed, a general method for complexity-regularized restoration remained as an open question for a long while until our recent preliminary publication [5], where we presented a generic and practical approach flexible in both the degradation model addressed and the compression technique utilized.

Our strategy for complexity-regularized signal restoration relies on the Half Quadratic Splitting approach (see other uses in [6], [7]), decomposing the difficult optimization problem into a sequence of easier tasks including ℓ_2 -regularized inverse problems and standard rate-distortion optimizations (with respect to a squared-error distortion metric). A main part of our methodology is to replace the rate-distortion optimization with standardized compression techniques enabling an indirect utilization of signal models used for efficient compression designs.

Our method relates to various contemporary concepts in signal and image processing. The recent frameworks of Plug-and-Play Priors [8] and Regularization-by-Denoising [9] suggest leveraging a Gaussian denoiser for more complicated restoration tasks, achieving impressive results (see, e.g., [8]–[12]). However, our method is not only the compression-based counterpart for denoising-based restoration concepts from [8], [9]. In fact we carry out restoration using a more elementary component – since compression can be directly used in the design of a Gaussian denoiser [1]–[3], but not the other way around. Denoising indeed makes signals more compressible but cannot be used in a straightforward way to do compression.

Commonly, compression methods process the given signal based on its decomposition into non-overlapping blocks, yielding block-level rate-distortion optimizations based on block bit-costs. The corresponding complexity measure sums the bit-costs of all the non-overlapping blocks, however, note that this evaluation is shift sensitive. This fact motivates us to propose a shift-invariant complexity regularizer by quantifying the bit-costs of all the overlapping blocks of the signal estimate. This improved regularizer calls for our restoration procedure to use averaging of decompressed signals obtained from compressions of shifted signals. Our shift-invariant approach conforms with the Expected Patch Log-Likelihood (EPLL) idea [7], where a full-signal regularizer is formed based on a

block-level prior in a way leading to averaging MAP estimates of shifted signal versions. Our extended method also recalls the cycle spinning concept, presented in [13] for wavelet-based denoising. Additional resemblance is to the compression postprocessing techniques in [14], [15] enhancing a given decompressed image by averaging supplementary compression-decompression results of shifted versions of the given image, thus, our method generalizes this approach to any restoration problem with an appropriate consideration of the degradation operator. Very recent works [16], [17] suggested the use of compression techniques for compressive sensing of signals and images, but our approach examines other perspectives and settings referring to restoration problems as will be explained below.

In this paper we extend our previous conference publication [5] with new theoretical and experimental results. In the theory section, we study the problem of complexity-regularized restoration of a cyclo-stationary Gaussian signal from a degradation procedure consisting of a linear shift-invariant operator and additive white Gaussian noise. We gradually establish a few equivalent optimization forms, emphasizing two main concepts for complexity-regularized restoration: the degraded signal should go through a simple inverse filtering procedure, and then should be compressed so that the decompression components will have a varying quality distribution determined by the degradation-filter energy-distribution. We explain how these ideas materialize in the practical approach we propose, thus, establishing a theoretical reasoning for the feasible complexity-regularized restoration.

In the experiments section we provide new results demonstrating the practical complexity-regularized restoration approach for image deblurring. While deblurring is a challenging restoration task, we present compelling results obtained using the image compression profile of the HEVC standard [18]. An objective comparison to other deblurring techniques showed that the proposed implementation is a very good, but not a leading deblurring method. Moreover, we also extend our evaluation given in [5] for image inpainting. Here, we use HEVC compression to restore images from a severe degradation of 80% missing pixels. Interestingly, our compression-based image inpainting approach can be perceived as the dual concept of inpainting-based compression of images and videos suggested in, e.g., [19]–[21].

This paper is organized as follows. In section II we overview the settings of the complexity-regularized restoration problem. In section III we present the proposed practical methods for complexity-regularized restoration. In section IV we theoretically analyze particular problem settings where the signal is a cyclo-stationary Gaussian process. In section V we provide experimental results for image deblurring and inpainting. Section VI concludes this paper.

II. COMPLEXITY-REGULARIZED RESTORATION: PROBLEM SETTINGS

A. Regularized Restoration of Signals

In this paper we address the task of restoring a signal $\mathbf{x}_0 \in \mathbb{R}^N$ from a degraded version, $\mathbf{y} \in \mathbb{R}^M$, obeying the prevalent deterioration model:

$$\mathbf{y} = \mathbf{H}\mathbf{x}_0 + \mathbf{n} \quad (1)$$

where \mathbf{H} is a $M \times N$ matrix being a linear degradation operator (e.g., blur, pixel omission, decimation) and $\mathbf{n} \in \mathbb{R}^M$ is a white Gaussian noise vector having zero mean and variance σ_n^2 .

Maximum A-Posteriori (MAP) estimation is a widely-known statistical approach forming the restored signal, $\hat{\mathbf{x}}$, via

$$\hat{\mathbf{x}} = \operatorname{argmax}_{\mathbf{x}} p(\mathbf{x}|\mathbf{y}) \quad (2)$$

where $p(\mathbf{x}|\mathbf{y})$ is the posterior probability. For the above defined degradation model (1), incorporating additive white Gaussian noise, the MAP estimate reduces to the form of

$$\hat{\mathbf{x}} = \operatorname{argmin}_{\mathbf{x}} \frac{1}{2\sigma_n^2} \|\mathbf{H}\mathbf{x} - \mathbf{y}\|_2^2 - \log p(\mathbf{x}) \quad (3)$$

where $p(\mathbf{x})$ is the prior probability that, here, evaluates the probability of the candidate solution.

Another prevalent restoration approach, embodied in many contemporary techniques, forms the estimate via the optimization

$$\hat{\mathbf{x}} = \operatorname{argmin}_{\mathbf{x}} \|\mathbf{H}\mathbf{x} - \mathbf{y}\|_2^2 + \mu s(\mathbf{x}) \quad (4)$$

where $s(\mathbf{x})$ is a general regularization function returning a lower value for a more likely candidate solution, and $\mu \geq 0$ is a parameter weighting the regularization effect. This strategy for restoration based on arbitrary regularizers can be interpreted as a generalization of the MAP approach in (3). Specifically, comparing the formulations (4) and (3) exhibits the regularization function $s(\mathbf{x})$ and the parameter μ as extensions of $(-\log p(\mathbf{x}))$ and the factor $2\sigma_n^2$, respectively.

Among the various regularization functions that can be associated with the general restoration approach in (4), we explore here the class of complexity regularizers measuring the required number of bits for the compressed representation of the candidate solution. The practical methods presented in this section focus on utilizing existing (independent) compression techniques, implicitly employing their underlying signal models for the restoration task.

B. Operational Rate-Distortion Optimization

The practical complexity-regularized restoration methods in this section are developed with respect to a compression technique obeying the following conceptual design. The signal is segmented to equally-sized non-overlapping blocks (each is consisted of N_b samples) that are independently compressed. The block compression procedure is modeled as a general variable-rate vector quantizer that employs a codebook, \mathcal{C} , allowing a finite set of block reconstruction candidates, each is associated with a binary codeword for its compressed

description. It is assumed that shorter codewords are coupled with block reconstructions that are, in general, more likely.

The signal \mathbf{x} is compressed based on its segmentation into a set of blocks $\{\mathbf{x}_i\}_{i \in \mathcal{B}}$ (where \mathcal{B} denotes the index set of blocks in the non-overlapping partitioning of the signal). In addition we introduce the function $r(\mathbf{z})$ that evaluates the bit-cost (i.e., the length of the binary codeword) for the block reconstruction $\mathbf{z} \in \mathcal{C}$. Then, the operational rate-distortion optimization corresponding to the described architecture and a squared-error distortion metric is

$$\{\tilde{\mathbf{x}}_i\}_{i \in \mathcal{B}} = \underset{\{\mathbf{v}_i\}_{i \in \mathcal{B}} \in \mathcal{C}}{\operatorname{argmin}} \sum_{i \in \mathcal{B}} \|\mathbf{x}_i - \mathbf{v}_i\|_2^2 + \lambda \sum_{i \in \mathcal{B}} r(\mathbf{v}_i), \quad (5)$$

where $\lambda \geq 0$ is a Lagrange multiplier corresponding to some total compression bit-cost. Importantly, the independent representation of non-overlapping blocks allows solving (5) separately for each block [22], [23].

Our mathematical developments require the following algebraic tools for block handling. The matrix \mathbf{P}_i is defined to provide the i^{th} block from the complete signal via the standard multiplication $\mathbf{P}_i \mathbf{x} = \mathbf{x}_i$. Note that \mathbf{P}_i can extract any block of the signal, even one that is not in the non-overlapping grid \mathcal{B} . Accordingly, the matrix \mathbf{P}_i^T locates a block in the i^{th} block-position in a construction of a full-sized signal and, therefore, lets to express the a complete signal as $\mathbf{x} = \sum_{i \in \mathcal{B}} \mathbf{P}_i^T \mathbf{x}_i$.

Now we can use the block handling operator \mathbf{P}_i for expressing the block-based rate-distortion optimization in its corresponding full-signal formulation:

$$\tilde{\mathbf{x}} = \underset{\mathbf{v} \in \mathcal{C}_{\mathcal{B}}}{\operatorname{argmin}} \|\mathbf{x} - \mathbf{v}\|_2^2 + \lambda r_{tot}(\mathbf{v}). \quad (6)$$

where $\mathcal{C}_{\mathcal{B}}$ is the full-signal codebook, being the discrete set of candidate reconstructions for the full signal, defined using the block-level codebook \mathcal{C} as

$$\mathcal{C}_{\mathcal{B}} = \left\{ \mathbf{v} \mid \mathbf{v} = \sum_{i \in \mathcal{B}} \mathbf{P}_i^T \mathbf{v}_i, \quad \{\mathbf{v}_i\}_{i \in \mathcal{B}} \in \mathcal{C} \right\}. \quad (7)$$

Moreover, the regularization function in (6) is the total bit cost of the reconstructed signal defined for $\mathbf{v} \in \mathcal{C}_{\mathcal{B}}$ as $r_{tot}(\mathbf{v}) \triangleq \sum_{i \in \mathcal{B}} r(\mathbf{P}_i \mathbf{v})$.

C. Complexity-Regularized Restoration: Basic Optimization Formulation

While the regularized-restoration optimization in (4) is over a continuous domain, the operational rate-distortion optimization in (6) is a discrete problem with solutions limited to the set $\mathcal{C}_{\mathcal{B}}$. Therefore, we extend the definition of the block bit-cost evaluation function such that it is defined for any $\mathbf{z} \in \mathbb{R}^{N_b}$ via

$$\bar{r}(\mathbf{z}) = \begin{cases} r(\mathbf{z}) & , \mathbf{z} \in \mathcal{C} \\ \infty & , \mathbf{z} \notin \mathcal{C} \end{cases}, \quad (8)$$

and the corresponding extension of the total bit-cost $\bar{r}_{tot}(\mathbf{x}) \triangleq \sum_{i \in \mathcal{B}} \bar{r}(\mathbf{P}_i \mathbf{x})$ is defined for any $\mathbf{x} \in \mathbb{R}^N$.

Now we define the complexity regularization function as

$$s(\mathbf{x}) = \bar{r}_{tot}(\mathbf{x}) \quad (9)$$

and the corresponding restoration optimization is

$$\hat{\mathbf{x}} = \underset{\mathbf{x}}{\operatorname{argmin}} \|\mathbf{Hx} - \mathbf{y}\|_2^2 + \mu \bar{r}_{tot}(\mathbf{x}). \quad (10)$$

Due to the definition of the extended bit-cost evaluation function, $\bar{r}_{tot}(\mathbf{x})$, the solution candidates of (10) are limited to the discrete set $\mathcal{C}_{\mathcal{B}}$ as defined in (7).

Examining the complexity-regularized restoration in (10) for the Gaussian denoising task, where $\mathbf{H} = \mathbf{I}$, shows that the optimization reduces to the regular rate-distortion optimization in (6), namely, the compression of the noisy signal \mathbf{y} . However, for more complicated restoration problems, where \mathbf{H} has an arbitrary structure, the optimization in (10) is not easy to solve and, in particular, it does not correspond to standard compression designs that are optimized for the regular squared-error distortion metric.

III. PROPOSED METHODS

In this section we present two restoration methods leveraging a given compression technique. The distinct algorithms result from two different definitions for the complexity regularization function. While the first approach regularizes the total bit-cost of the non-overlapping blocks of the restored signal, the second refers to the total bit-cost of all the overlapping blocks of the estimate.

A. Regularize Total Complexity of Non-Overlapping Blocks

Here we establish a practical method addressing the optimization problem in (10) based on the Half Quadratic Splitting approach (for additional uses see, e.g., [7]). The optimization (10) can be expressed also as

$$\hat{\mathbf{x}} = \underset{\mathbf{x}}{\operatorname{argmin}} \|\mathbf{Hx} - \mathbf{y}\|_2^2 + \mu \sum_{i \in \mathcal{B}} \bar{r}(\mathbf{P}_i \mathbf{x}), \quad (11)$$

where the degradation matrix \mathbf{H} , having a general structure, renders a block-based treatment infeasible.

Addressing this structural difficulty using the Half Quadratic Splitting strategy begins with introducing the auxiliary variables $\{\mathbf{z}_i\}_{i \in \mathcal{B}}$, where \mathbf{z}_i is coupled with the i^{th} non-overlapping block. Specifically, we reformulate the problem (11) into

$$\begin{aligned} (\hat{\mathbf{x}}, \{\hat{\mathbf{z}}_i\}_{i \in \mathcal{B}}) = & \underset{\mathbf{x}, \{\mathbf{z}_i\}_{i \in \mathcal{B}}}{\operatorname{argmin}} \|\mathbf{Hx} - \mathbf{y}\|_2^2 + \mu \sum_{i \in \mathcal{B}} \bar{r}(\mathbf{z}_i) \\ \text{s.t.} \quad \mathbf{z}_i &= \mathbf{P}_i \mathbf{x} \quad , \text{for } i \in \mathcal{B}. \end{aligned} \quad (12)$$

A relaxed form of the constrained optimization (12) is constructed by translating the equality constraints to a quadratic penalty terms in the following unconstrained form of the problem:

$$\begin{aligned} (\hat{\mathbf{x}}, \{\hat{\mathbf{z}}_i\}_{i \in \mathcal{B}}) = & \underset{\mathbf{x}, \{\mathbf{z}_i\}_{i \in \mathcal{B}}}{\operatorname{argmin}} \|\mathbf{Hx} - \mathbf{y}\|_2^2 + \\ & \frac{\beta}{2} \sum_{i \in \mathcal{B}} \|\mathbf{P}_i \mathbf{x} - \mathbf{z}_i\|_2^2 + \mu \sum_{i \in \mathcal{B}} \bar{r}(\mathbf{z}_i), \end{aligned} \quad (13)$$

where $\beta > 0$ is a parameter controlling the closeness of each \mathbf{z}_i to its counterpart variable $\mathbf{P}_i \mathbf{x}$. Hence, the constraints in (12) are more closely approximated for larger β .

Each of the optimization variables in (13) participates only in two of the three terms in the cost function and, therefore, we employ alternating minimization to obtain an iterative solution consisted of simpler optimizations. Similar to [7], the β parameter is gradually increased along the iterations and set to empirically-defined values yielding convergence to a solution that approximately satisfies the constraints in (12). Accordingly, the t^{th} iteration of the proposed iterative solution is

$$\hat{\mathbf{x}}^{(t)} = \underset{\mathbf{x}}{\operatorname{argmin}} \|\mathbf{H}\mathbf{x} - \mathbf{y}\|_2^2 + \frac{\beta^{(t)}}{2} \sum_{i \in \mathcal{B}} \|\mathbf{P}_i \mathbf{x} - \hat{\mathbf{z}}_i^{(t-1)}\|_2^2 \quad (14)$$

$$\hat{\mathbf{z}}_i^{(t)} = \underset{\mathbf{z}_i}{\operatorname{argmin}} \frac{\beta^{(t)}}{2} \|\mathbf{P}_i \hat{\mathbf{x}}^{(t)} - \mathbf{z}_i\|_2^2 + \mu \bar{r}(\mathbf{z}_i), \quad i \in \mathcal{B} \quad (15)$$

$$\text{Set } \beta^{(t+1)} \text{ as an increment of } \beta^{(t)}. \quad (16)$$

The analytic solution of the first stage optimization in (14) is

$$\hat{\mathbf{x}}^{(t)} = \left(\mathbf{H}^T \mathbf{H} + \frac{\beta^{(t)}}{2} \mathbf{I} \right)^{-1} \left(\mathbf{H}^T \mathbf{y} + \frac{\beta^{(t)}}{2} \sum_{i \in \mathcal{B}} \mathbf{P}_i^T \hat{\mathbf{z}}_i^{(t-1)} \right) \quad (17)$$

rendering this stage as a weighted averaging of the deteriorated signal with the block estimates obtained in the second stage of the previous iteration.

The optimizations in the second stage of each iteration (15) are rate-distortion optimizations corresponding to each of the non-overlapping blocks of the signal estimate $\hat{\mathbf{x}}^{(t)}$ obtained in the first stage. Accordingly, the set of block-level optimizations in (15) can be interpreted as a single full-signal rate-distortion optimization with respect to a Lagrange multiplier value of $\lambda^{(t)} = \frac{2\mu}{\beta^{(t)}}$. Interestingly, since $\beta^{(t)}$ is increased in each iteration (see (16)), the Lagrangian multiplier value decreases correspondingly – thus relaxing the compression bit-cost constraint. We denote the compression-decompression procedure that replaces (15) as

$$\hat{\mathbf{z}}^{(t)} = \operatorname{CompressDecompress}_{\lambda^{(t)}}(\hat{\mathbf{x}}^{(t)}), \quad (18)$$

where $\hat{\mathbf{z}}^{(t)}$ is the decompressed signal assembled from the non-overlapping decompressed blocks.

We further suggest using a standardized compression method as the compression-decompression operator (18). While many compression methods do not follow the exact rate-distortion optimizations we have in our mathematical development, we still encourage utilizing such techniques as an approximation for (15). Additionally, since many compression methods do not rely on Lagrangian optimization, their operating parameters may have different definitions such as quality parameters, compression ratios, or output bit-rates. Accordingly, we present the suggested algorithm with respect to a general compression-decompression procedure with output bit-cost directly or indirectly affected by a parameter denoted

as θ . Without loss of generality, we consider that the reduction of θ increases the output bit-cost (similarly to the Lagrangian multiplier role in (15)). Hence, the iteration update of θ obeys $\theta^{(t+1)} < \theta^{(t)}$. One should also note that in the general case β and θ are independently updated since they do not have a formally defined relation. These generalizations are also implemented in the proposed Algorithm 1.

Importantly, Algorithm 1 does not only restore the deteriorated input image, but also provides the signal estimate in a compressed form by employing the output of the compression stage of the last iteration.

Algorithm 1 Proposed Method Based on Total Complexity of Non-Overlapping Blocks

- 1: Initialize $\hat{\mathbf{z}}^{(0)}$ (depending on the deterioration type).
- 2: $t = 1, \beta^{(1)} = \beta_1, \theta^{(1)} = \theta_1$
- 3: **repeat**
- 4: $\hat{\mathbf{x}}^{(t)} = \left(\mathbf{H}^T \mathbf{H} + \frac{\beta^{(t)}}{2} \mathbf{I} \right)^{-1} \left(\mathbf{H}^T \mathbf{y} + \frac{\beta^{(t)}}{2} \hat{\mathbf{z}}^{(t-1)} \right)$
- 5: $\hat{\mathbf{z}}^{(t)} = \operatorname{CompressDecompress}_{\theta^{(t)}}(\hat{\mathbf{x}}^{(t)})$.
- 6: Set $\beta^{(t+1)}$ as an increment of $\beta^{(t)}$
- 7: Set $\theta^{(t+1)}$ as a decrease of $\theta^{(t)}$
- 8: $t \leftarrow t + 1$
- 9: **until** stopping criterion is satisfied

B. Regularize Total Complexity of All Overlapping Blocks

Algorithm 1 emerged from complexity regularization measuring the total bit-cost of the estimate based on its decomposition into non-overlapping blocks (see Eq. (11)), resulting in a restored signal available in a compressed form compatible with the compression technique in use. Obviously, the above approach provides estimates limited to the discrete set of signals supported by the compression architecture, thus, having a somewhat reduced restoration ability with respect to methods providing estimates from an unrestricted domain of solutions. This observation motivates us to develop a complexity-regularized restoration procedure that provides good estimates from the continuous unrestricted domain of signals while still utilizing a standardized compression technique as its main component.

As before, our developments refer to a general block-based vector quantizer relying on a codebook \mathcal{C} as a discrete set of block-reconstruction candidates. We consider here the segmentation of the signal-block space, \mathbb{R}^{N_b} , given by the voronoi cells corresponding to the compression reconstruction candidates, namely, for each $\mathbf{c} \in \mathcal{C}$ there is a region

$$V_{\mathbf{c}} \triangleq \left\{ \mathbf{w} \in \mathbb{R}^{N_b} \mid \mathbf{c} = \arg \min_{\tilde{\mathbf{c}} \in \mathcal{C}} \|\mathbf{w} - \tilde{\mathbf{c}}\|_2^2 \right\} \quad (19)$$

defining all the vectors in \mathbb{R}^{N_b} that \mathbf{c} is their nearest member of \mathcal{C} . We use the voronoi cells in (19) for defining an alternative extension to the bit-cost evaluation of a signal block (i.e., the new definition, $\bar{r}_v(\mathbf{z})$, will replace $\bar{r}(\mathbf{z})$ given in (8) that was used for the development of Algorithm 1). Specifically, we

associate a finite bit-cost to any $\mathbf{z} \in \mathbb{R}^{N_b}$ based on the voronoi cell it resides in, i.e.,

$$\bar{r}_v(\mathbf{z}) = r(\mathbf{c}) \text{ for } \mathbf{z} \in V_{\mathbf{c}} \quad (20)$$

where $r(\mathbf{c})$ is the regular bit-cost evaluation defined in Section II-B only for blocks in \mathcal{C} .

The method proposed here emerges from a new complexity regularization function that quantifies the total complexity of all the overlapping blocks of the estimate. Using the extended bit-cost measure $\bar{r}_v(\cdot)$, defined in (20), we introduce the full-signal regularizer as

$$s^*(\mathbf{x}) = \sum_{i \in \mathcal{B}^*} \bar{r}_v(\mathbf{P}_i \mathbf{x}) \quad (21)$$

where $\mathbf{x} \in \mathbb{R}^N$, and \mathcal{B}^* is a set containing the indices of all the overlapping blocks of the signal. The associated restoration optimization is

$$\hat{\mathbf{x}} = \underset{\mathbf{x}}{\operatorname{argmin}} \|\mathbf{H}\mathbf{x} - \mathbf{y}\|_2^2 + \mu \sum_{i \in \mathcal{B}^*} \bar{r}_v(\mathbf{P}_i \mathbf{x}). \quad (22)$$

Importantly, in contrast to the previous subsection, the function $s^*(\mathbf{x})$ evaluates the complexity of any $\mathbf{x} \in \mathbb{R}^N$ with a finite value and, thus, does not restrict the restoration to the discrete set of codebook-based constructions, $\mathcal{C}_{\mathcal{B}}$, defined in (7).

While the new regularizer in (22) is not separable into complexity evaluation of non-overlapping blocks, the Half Quadratic Splitting approach can accommodate it as well. This is explained next. We define the auxiliary variables $\{\mathbf{z}_i\}_{i \in \mathcal{B}^*}$, where each \mathbf{z}_i is coupled with the i^{th} overlapping block. Then, the optimization (22) is expressed as

$$\begin{aligned} (\hat{\mathbf{x}}, \{\hat{\mathbf{z}}_i\}_{i \in \mathcal{B}^*}) &= \underset{\mathbf{x}, \{\mathbf{z}_i\}_{i \in \mathcal{B}^*}}{\operatorname{argmin}} \|\mathbf{H}\mathbf{x} - \mathbf{y}\|_2^2 + \mu \sum_{i \in \mathcal{B}^*} \bar{r}_v(\mathbf{z}_i) \\ \text{s.t.} \quad \mathbf{z}_i &= \mathbf{P}_i \mathbf{x} \quad \text{for } i \in \mathcal{B}^*. \end{aligned} \quad (23)$$

As in Section III-A, we replace the equality constraints with quadratic penalties, employ alternating minimization, resulting in an iterative solution provided by the following three steps in each iteration (as before t denotes the iteration number):

$$\hat{\mathbf{x}}^{(t)} = \underset{\mathbf{x}}{\operatorname{argmin}} \|\mathbf{H}\mathbf{x} - \mathbf{y}\|_2^2 + \frac{\beta^{(t)}}{2} \sum_{i \in \mathcal{B}^*} \left\| \mathbf{P}_i \mathbf{x} - \hat{\mathbf{z}}_i^{(t-1)} \right\|_2^2 \quad (24)$$

$$\hat{\mathbf{z}}_i^{(t)} = \underset{\mathbf{z}_i}{\operatorname{argmin}} \frac{\beta^{(t)}}{2} \left\| \mathbf{P}_i \hat{\mathbf{x}}^{(t)} - \mathbf{z}_i \right\|_2^2 + \mu \bar{r}_v(\mathbf{z}_i), \quad i \in \mathcal{B}^* \quad (25)$$

$$\text{Set } \beta^{(t+1)} \text{ as an increment of } \beta^{(t)}. \quad (26)$$

While the procedure above resembles the one from the former subsection, the treatment of overlapping blocks has different interpretations to the optimizations in (24) and (25). Indeed, note that the block-level rate-distortion optimizations in (25) are not discrete due to the extended bit-cost evaluation $\bar{r}_v(\cdot)$ defined in (20). Due to the definition of $\bar{r}_v(\cdot)$, the rate-distortion optimizations (25) can be considered as continuous relaxations of the discrete optimizations done by the practical compression technique. Since we intend using a given compression method without explicit knowledge of its underlying codebook, we cannot construct the voronoi cells defining

$\bar{r}_v(\cdot)$ and, thus, it is impractical to accurately solve (25). Consequently, we suggest to approximate the optimizations (25) by the discrete forms of

$$\hat{\mathbf{z}}_i^{(t)} = \underset{\mathbf{z}_i}{\operatorname{argmin}} \frac{\beta^{(t)}}{2} \left\| \mathbf{P}_i \hat{\mathbf{x}}^{(t)} - \mathbf{z}_i \right\|_2^2 + \mu \bar{r}(\mathbf{z}_i), \quad i \in \mathcal{B}^* \quad (27)$$

where $\bar{r}(\cdot)$ is the discrete evaluation of the block bit-cost, defined in (8), letting to identify the problems as operational rate-distortion optimizations of the regular discrete form.

Each block-level rate-distortion optimization in (27) is associated with each one of the overlapping blocks of the signal. Accordingly, we interpret this group of optimizations as multiple applications of a full-signal compression-decompression procedure, each associates to a shifted version of the signal (corresponding to different sets of non-overlapping blocks). Specifically, for a signal \mathbf{x} and a compression block-size of N_b samples, there are N_b shifted grids of non-overlapping blocks. For mathematical convenience, we consider here cyclic shifts such that the j^{th} shift ($j = 1, \dots, N_b$) corresponds to a signal of N samples taken cyclically starting at the j^{th} sample of \mathbf{x} (in practice other definitions of shifts may be used, e.g., see Section V for a suggested treatment of two-dimensional signals). We denote the j^{th} shifted signal as $\text{shift}_j \{\mathbf{x}\}$. Moreover, we denote the index set of blocks included in the j^{th} shifted signal as \mathcal{B}^j (noting that $\mathcal{B}^1 = \mathcal{B}$), hence, $\mathcal{B}^* = \bigcup_{j=1}^{N_b} \mathcal{B}^j$. Therefore, the decompressed blocks $\{\hat{\mathbf{z}}_i^{(t)}\}_{i \in \mathcal{B}^*}$ can be obtained by multiple full-signal compression-decompression applications, namely, $\hat{\mathbf{z}}^{j,(t)} = \text{CompressDecompress}_{\lambda}(\text{shift}_j \{\hat{\mathbf{x}}^{(t)}\})$ for $j = 1, \dots, N_b$, where the Lagrangian multiplier value is $\lambda = \frac{2\mu}{\beta^{(t)}}$. The j^{th} decompressed image, $\hat{\mathbf{z}}^{j,(t)}$, is composed of the blocks $\{\hat{\mathbf{z}}_i^{(t)}\}_{i \in \mathcal{B}^j}$ that can be obtained via

$$\hat{\mathbf{z}}_i^{(t)} = \mathbf{P}_i \text{shift}_j^{-1} \{\hat{\mathbf{z}}^{j,(t)}\} \quad \text{for } i \in \mathcal{B}^j \quad (28)$$

where $\text{shift}_j^{-1} \{\cdot\}$ is the inverse shift operator that (cyclically) shifts back the given full-size signal by j samples.

The analytic solution of the optimization (24) is

$$\begin{aligned} \hat{\mathbf{x}}^{(t)} &= \left(\mathbf{H}^T \mathbf{H} + \frac{\beta^{(t)}}{2} \sum_{i \in \mathcal{B}^*} \mathbf{P}_i^T \mathbf{P}_i \right)^{-1} \\ &\quad \times \left(\mathbf{H}^T \mathbf{y} + \frac{\beta^{(t)}}{2} \sum_{i \in \mathcal{B}^*} \mathbf{P}_i^T \hat{\mathbf{z}}_i^{(t-1)} \right), \end{aligned} \quad (29)$$

showing that the first stage of each iteration is a weighted averaging of the given deteriorated signal with all the overlapping decompressed blocks obtained in the former iteration. Note that $\sum_{i \in \mathcal{B}^*} \mathbf{P}_i^T \mathbf{P}_i$ is a diagonal matrix, where its (k, k) component evaluates the number of decompressed blocks that the k^{th} signal sample is involved in. Additionally, the averaging in (29) can be directly applied on the full decompressed signals $\hat{\mathbf{z}}^{j,(t)}$ ($j = 1, \dots, N_b$) after appropriate inverse shifts as suggested in Algorithm 2, where we denote the sum of

decompressed signals as

$$\hat{\mathbf{z}}_{sum}^{(t)} \triangleq \sum_{j=1}^{N_b} \left(\sum_{i \in \mathcal{B}^j} \mathbf{P}_i^T \mathbf{P}_i \right) shift_j^{-1} \left\{ \hat{\mathbf{z}}^{j,(t)} \right\}. \quad (30)$$

Algorithm 2 summarizes the practical restoration method for a compression technique operated by the general parameter θ for determining the bit-cost (see details in Section III-A).

Algorithm 2 Proposed Method Based on Total Complexity of All the Overlapping Blocks

- 1: Initialize $\hat{\mathbf{z}}_{sum}^{(0)}$ (depending on the deterioration type).
- 2: $t = 1$, $\beta^{(1)} = \beta_1$, $\theta^{(1)} = \theta_1$
- 3: **repeat**
- 4: $\hat{\mathbf{x}}^{(t)} = \left(\mathbf{H}^T \mathbf{H} + \frac{\beta^{(t)}}{2} \sum_{i \in \mathcal{B}^*} \mathbf{P}_i^T \mathbf{P}_i \right)^{-1} \times \left(\mathbf{H}^T \mathbf{y} + \frac{\beta^{(t)}}{2} \hat{\mathbf{z}}_{sum}^{(t-1)} \right)$
- 5: $\hat{\mathbf{z}}^{j,(t)} = CompressDecompress_{\theta^{(t)}} \left(shift_j \left\{ \hat{\mathbf{x}}^{(t)} \right\} \right)$, $(j = 1, \dots, N_b)$.
- 6: $\hat{\mathbf{z}}_{sum}^{(t)} = \sum_{j=1}^{N_b} \left(\sum_{i \in \mathcal{B}^j} \mathbf{P}_i^T \mathbf{P}_i \right) shift_j^{-1} \left\{ \hat{\mathbf{z}}^{j,(t)} \right\}$
- 7: Set $\beta^{(t+1)}$ as an increment of $\beta^{(t)}$
- 8: Set $\theta^{(t+1)}$ as a decrease of $\theta^{(t)}$
- 9: $t \leftarrow t + 1$
- 10: **until** stopping criterion is satisfied

IV. RATE-DISTORTION THEORETIC ANALYSIS FOR THE GAUSSIAN CASE

In this section we theoretically study the complexity-regularized restoration problem from the perspective of rate-distortion theory. While our analysis is focused on the particular settings of a cyclo-stationary Gaussian signal and deterioration caused by a linear shift-invariant operator and additive white Gaussian noise, the results clearly explain the main principles of complexity-regularized restoration.

Consider the signal $\mathbf{x} \in \mathbb{R}^N$ modeled as a zero-mean Gaussian random vector with autocorrelation matrix \mathbf{R}_x , i.e., $\mathbf{x} \sim \mathcal{N}(0, \mathbf{R}_x)$. The degradation model studied remains

$$\mathbf{y} = \mathbf{Hx} + \mathbf{n}, \quad (31)$$

where here \mathbf{H} is a real-valued $N \times N$ circulant matrix representing a linear shift-invariant deteriorating operation and $\mathbf{n} \sim \mathcal{N}(0, \sigma_n^2 \mathbf{I})$ is a length N vector of white Gaussian noise. Clearly, the degraded observation \mathbf{y} is also a zero-mean Gaussian random vector with autocorrelation matrix $\mathbf{R}_y = \mathbf{H} \mathbf{R}_x \mathbf{H}^* + \sigma_n^2 \mathbf{I}$.

A. Prevalent Restoration Strategies

We precede the analysis of the complexity-regularized restoration with mentioning three well-known estimation methods. The restoration procedure is a function

$$\hat{\mathbf{x}} = f(\mathbf{y}), \quad (32)$$

where f maps the degraded signal \mathbf{y} to an estimate of \mathbf{x} denoted as $\hat{\mathbf{x}}$. In practice, one gets a realization of \mathbf{y} denoted here as \mathbf{y}_r and forms the corresponding estimate as $\hat{\mathbf{x}}_r = f(\mathbf{y}_r)$.

1) *Minimum Mean Squared Error (MMSE) Estimate*: This restoration minimizes the expected MSE of the estimate, i.e.,

$$f_{MMSE} = \underset{f}{\operatorname{argmin}} E \left\{ (\mathbf{x} - f(\mathbf{y}))^2 \right\}, \quad (33)$$

yielding that the corresponding estimate is the conditional expectation of \mathbf{x} given \mathbf{y}

$$\hat{\mathbf{x}}_{MMSE} = f_{MMSE}(\mathbf{y}) = E \{ \mathbf{x} | \mathbf{y} \}. \quad (34)$$

Nicely, for the Gaussian case considered in this section, the MMSE estimate (34) reduces to a linear operator, presented below as the Wiener filter.

2) *Wiener Filtering*: The Wiener filter is also known as the Linear Minimum Mean Squared Error (LMMSE) estimate, corresponding to a restoration function of the form

$$\hat{\mathbf{x}} = f_{Wiener}(\mathbf{y}) = \mathbf{A}\mathbf{y} + \mathbf{b}, \quad (35)$$

optimized via

$$\left\{ \hat{\mathbf{A}}, \hat{\mathbf{b}} \right\} = \underset{\mathbf{A}, \mathbf{b}}{\operatorname{argmin}} E \left\{ (\mathbf{x} - (\mathbf{A}\mathbf{y} + \mathbf{b}))^2 \right\}. \quad (36)$$

In our case, where \mathbf{x} and \mathbf{y} are zero mean, $\hat{\mathbf{b}} = \mathbf{0}$ and

$$\hat{\mathbf{A}} = \mathbf{R}_x \mathbf{H}^* \left(\mathbf{H} \mathbf{R}_x \mathbf{H}^* + \sigma_n^2 \mathbf{I} \right)^{-1}. \quad (37)$$

If the distributions are Gaussian, this linear operator coincides with the optimal MMSE estimator.

3) *Constrained Deconvolution Filtering*: This approach considers a given degraded signal $\mathbf{y}_r = \mathbf{Hx} + \mathbf{n}_r$, with the noise vector a realization of a random process while the signal \mathbf{x} is considered as a deterministic vector, with perhaps some known properties. Then, the restoration is carried out by minimizing a carefully-designed penalty function, g , that assumes lower values for \mathbf{x} vectors that fit the prior knowledge on \mathbf{x} . The estimate is constrained to conform with the known degradation model (31), by demanding the similarity of $\mathbf{y}_r - \mathbf{H}\hat{\mathbf{x}}$ to the additive noise term. These two requirements are implemented in an optimization of the form

$$\begin{aligned} \min_{\hat{\mathbf{x}}} \quad & g(\hat{\mathbf{x}}) \\ \text{subject to} \quad & \|\mathbf{y}_r - \mathbf{H}\hat{\mathbf{x}}\|_2^2 = N\sigma_n^2. \end{aligned} \quad (38)$$

Our practical methods presented in Section III emerge from an instance of the constrained deconvolution optimization (38), in its Lagrangian version, where the penalty function g is the cost in bits measuring the complexity in describing the estimate $\hat{\mathbf{x}}$. In the remaining of this section, we study the complexity-regularized restoration problem from a statistical perspective.

B. The Complexity-Regularized Restoration Problem and its Equivalent Forms

Based on rate-distortion theory (e.g., see [24]), we consider the estimate of \mathbf{x} as a random vector $\hat{\mathbf{x}} \in \mathbb{R}^N$ with the probability density function (PDF) $p_{\hat{\mathbf{x}}}(\hat{x})$. The estimate characterization, $p_{\hat{\mathbf{x}}}(\hat{x})$, is determined by optimizing the conditional PDF $p_{\hat{\mathbf{x}}|\mathbf{y}}(\hat{x}|y)$, statistically representing the mapping between the given data \mathbf{y} and the decompression result $\hat{\mathbf{x}}$. Moreover, the rate is measured as the mutual information between $\hat{\mathbf{x}}$ and \mathbf{y} , defined via

$$I(\mathbf{y}, \hat{\mathbf{x}}) = \int p_{\mathbf{y}, \hat{\mathbf{x}}}(y, \hat{x}) \log \frac{p_{\mathbf{y}, \hat{\mathbf{x}}}(y, \hat{x})}{p_{\mathbf{y}}(y) p_{\hat{\mathbf{x}}}(\hat{x})} dy d\hat{x}. \quad (39)$$

Then, the basic form of the complexity-regularized restoration optimization is expressed as

Problem 1 (Basic Form):

$$\begin{aligned} \min_{p_{\hat{\mathbf{x}}|\mathbf{y}}} \quad & I(\mathbf{y}, \hat{\mathbf{x}}) \\ \text{subject to} \quad & E \left\{ \|\mathbf{y} - \mathbf{H}\hat{\mathbf{x}}\|_2^2 \right\} = N\sigma_n^2. \end{aligned} \quad (40)$$

Here the estimate rate is minimized while maintaining suitability to the degradation model (31) using a distortion constraint set to achieve an a-priori known total noise energy. In general, Problem 1 is complicated to solve since the distortion constraint considers $\hat{\mathbf{x}}$ through the degradation operator \mathbf{H} , while the rate is directly evaluated for $\hat{\mathbf{x}}$.

The shift invariant operator \mathbf{H} is a circulant $N \times N$ matrix, thus, diagonalized by the $N \times N$ Discrete Fourier Transform (DFT) matrix \mathbf{F} . The (k, l) component of the DFT matrix ($k, l = 0, \dots, N-1$) is $\mathbf{F}_{k,l} = W_N^{kl}$ where $W_N \triangleq \frac{1}{\sqrt{N}} e^{-i2\pi k/N}$. Then, the diagonalization of \mathbf{H} is expressed as

$$\mathbf{F}\mathbf{H}\mathbf{F}^* = \Lambda_H, \quad (41)$$

where Λ_H is a diagonal matrix formed by the components h_k^F for $k = 0, \dots, N-1$. Using Λ_H we define the pseudoinverse of \mathbf{H} as

$$\mathbf{H}^+ = \mathbf{F}^* \Lambda_H^+ \mathbf{F}, \quad (42)$$

where Λ_H^+ is the pseudoinverse of Λ_H , an $N \times N$ diagonal matrix with the k^{th} diagonal element:

$$h_k^{F,+} = \begin{cases} \frac{1}{h_k^F}, & \text{for } h_k^F \neq 0 \\ 0, & \text{for } h_k^F = 0. \end{cases} \quad (43)$$

We denote by N_H the number of nonzero diagonal elements in Λ_H , the rank of \mathbf{H} .

The first main result of our analysis states that Problem 1, being the straightforward formulation for complexity-regularized restoration, is equivalent to the next problem.

Problem 2 (Pseudoinverse-filtered input):

$$\begin{aligned} \min_{p_{\hat{\mathbf{x}}|\tilde{\mathbf{y}}}} \quad & I(\tilde{\mathbf{y}}, \hat{\mathbf{x}}) \\ \text{subject to} \quad & E \left\{ \|\mathbf{H}(\tilde{\mathbf{y}} - \hat{\mathbf{x}})\|_2^2 \right\} = N_H \sigma_n^2, \end{aligned} \quad (44)$$

where

$$\tilde{\mathbf{y}} = \mathbf{H}^+ \mathbf{y} \quad (45)$$

is the pseudoinverse filtered version of the given degraded signal \mathbf{y} . One should note that Problem 2 has a more convenient form than Problem 1 since the distortion is an expected weighted squared error between the two random variables determining the rate. The equivalence of Problems 1 and 2 is proved in Appendix A.

In this section, \mathbf{x} is a cyclo-stationary Gaussian signal, hence, having a circulant autocorrelation matrix \mathbf{R}_x . Consequently, and also because \mathbf{H} is circulant, the deteriorated signal \mathbf{y} is also a cyclo-stationary Gaussian signal. Moreover, \mathbf{H}^+ is also a circulant matrix, thus, by (45) the pseudoinverse filtering result, $\tilde{\mathbf{y}}$, is also cyclo-stationary and zero-mean Gaussian. Specifically, the autocorrelation matrix of $\tilde{\mathbf{y}}$ is

$$\mathbf{R}_{\tilde{\mathbf{y}}} = \mathbf{H}^+ \mathbf{R}_y \mathbf{H}^{+*} \quad (46)$$

$$= \mathbf{H}^+ \mathbf{H} \mathbf{R}_x \mathbf{H}^{+*} \mathbf{H}^{+*} + \sigma_n^2 \mathbf{H}^+ \mathbf{H}^{+*}, \quad (47)$$

and, as a circulant matrix, it is diagonalized by the DFT matrix yielding the eigenvalues

$$\lambda_k^{(\tilde{\mathbf{y}})} = \begin{cases} \lambda_k^{(\mathbf{x})} + \frac{\sigma_n^2}{|h_k^F|^2}, & \text{for } h_k^F \neq 0 \\ 0, & \text{for } h_k^F = 0. \end{cases} \quad (48)$$

The DFT-domain representation of $\tilde{\mathbf{y}}$ is

$$\tilde{\mathbf{y}}^F = \mathbf{F} \tilde{\mathbf{y}}, \quad (49)$$

consisted of the coefficients $\{\tilde{y}_k^F\}_{k=0}^{N-1}$, being independent zero-mean Gaussian variables with variances corresponding to the eigenvalues in (48).

Transforming Problem 2 to the DFT domain, where $\tilde{\mathbf{y}}$ becomes a set of independent Gaussian variables to be coded under a joint distortion constraint, simplifies the optimization structure to the following separable form (see proof sketch in Appendix B).

Problem 3 (Separable form in DFT domain):

$$\begin{aligned} \min_{\left\{ p_{\hat{x}_k^F | \tilde{y}_k^F} \right\}_{k=0}^{N-1}} \quad & \sum_{k=0}^{N-1} I(\tilde{y}_k^F, \hat{x}_k^F) \\ \text{subject to} \quad & \sum_{k=0}^{N-1} |h_k^F|^2 E \left\{ |\tilde{y}_k^F - \hat{x}_k^F|^2 \right\} = N_H \sigma_n^2, \end{aligned} \quad (50)$$

where $\{\hat{x}_k^F\}_{k=0}^{N-1}$ are the elements of $\hat{\mathbf{x}}^F = \mathbf{F} \hat{\mathbf{x}}$. Nicely, the separable distortion in Problem 3 considers each variable using a squared error that is weighted by the squared magnitude of the corresponding degradation-filter coefficient.

The rate-distortion function of a single Gaussian variable with variance σ^2 has the known formulation [24]:

$$R(D) = \left[\frac{1}{2} \log \left(\frac{\sigma^2}{D} \right) \right]_+ \quad (51)$$

evaluating the minimal rate for a squared-error allowed reaching up to $D \geq 0$. In addition, the operator $[\cdot]_+$ is defined for real scalars as $[\alpha]_+ \triangleq \max\{\alpha, 0\}$, hence, $R(D) = 0$

for $D \geq \sigma^2$. Accordingly, the rate-distortion function of the Gaussian variable \tilde{y}_k^F is

$$R_k(D_k) = \left[\frac{1}{2} \log \left(\frac{\lambda_k^{(\tilde{y})}}{D_k} \right) \right]_+ \quad (52)$$

where D_k denotes the maximal squared-error allowed for this component. Now, similar to the famous case of jointly coding independent Gaussian variables with respect to a regular (non-weighted) squared-error distortion [24], we explicitly express Problem 3 as the following distortion-allocation optimization.

Problem 4 (Explicit distortion allocation):

$$\begin{aligned} & \min_{D_0, \dots, D_{N-1}} \sum_{k=0}^{N-1} \left[\frac{1}{2} \log \left(\frac{\lambda_k^{(\tilde{y})}}{D_k} \right) \right]_+ \\ & \text{subject to} \quad \sum_{k=0}^{N-1} |h_k^F|^2 D_k = N_H \sigma_n^2 \\ & \quad D_k \geq 0, \quad k = 0, \dots, N-1. \end{aligned} \quad (53)$$

The optimal distortion-allocation satisfying the last optimization is

$$D_k^{opt} = \begin{cases} \frac{\sigma_n^2}{|h_k^F|^2}, & \text{for } h_k^F \neq 0 \\ 0, & \text{for } h_k^F = 0 \end{cases} \quad (54)$$

and the associated optimal rates are

$$R_k^{opt} = \begin{cases} \frac{1}{2} \log \left(|h_k^F|^2 \frac{\lambda_k^{(\tilde{y})}}{\sigma_n^2} + 1 \right), & \text{for } h_k^F \neq 0 \\ 0, & \text{for } h_k^F = 0. \end{cases} \quad (55)$$

Results (54) and (55) are proved in Appendix C.

C. Demonstration of The Explicit Results

Let us exemplify the optimal rate-distortion results (54)-(55) for a cyclo-stationary Gaussian signal, \mathbf{x} , having the circulant autocorrelation matrix presented in Fig. 1a, corresponding to the eigenvalues $\{\lambda_k^{(\mathbf{x})}\}_{k=0}^{N-1}$ (Fig. 1b) obtained by a DFT-based decomposition. We first examine the denoising problem, where the signal-domain degradation matrix is $\mathbf{H} = \mathbf{I}$ (Fig. 2a) and its respective DFT-domain spectral representation is consisted of $h_k^F = 1$ for any k (see Fig. 2b). The additive white Gaussian noise has a sample variance of $\sigma_n^2 = 5$. Fig. 2c exhibits the optimal distortion allocation using a reverse-waterfilling diagram, where the signal-energy distribution $\{\lambda_k^{(\mathbf{x})}\}_{k=0}^{N-1}$ (black solid line) and the additive noise energy (the light-red region) defining together the noisy-signal energy level (purple solid line) corresponding to $\lambda_k^{(\tilde{y})} = \lambda_k^{(\mathbf{x})} + \sigma_n^2$. The blue dashed line in Fig. 2c shows the water level associated with the uniform distortion allocation. The optimal rate-allocation, corresponding to Fig. 2c and Eq. (55), is presented in Fig. 2d showing that more bits are spent on components with higher signal-to-noise ratios.

Another example considers the same Gaussian signal described in Fig. 1 and the noise level of $\sigma_n^2 = 5$, but here the degradation operator is the circulant matrix shown in Fig. 3a having a DFT-domain representation given in magnitude-levels in Fig. 3b exhibiting its frequency attenuation and

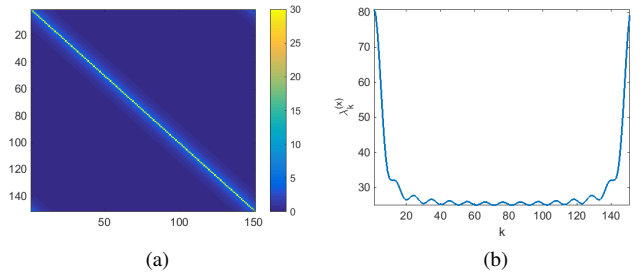


Fig. 1. The autocorrelation of the cyclo-stationary Gaussian signal used in the demonstration. (a) The circulant autocorrelation matrix in the signal domain, and (b) the corresponding eigenvalues obtained using the DFT decomposition.

amplification effects. The waterfilling diagram in Fig. 3c includes the same level of signal energy (black solid line) as in the denoising experiment, but the effective additive noise levels and the allocated distortions are clearly modulated in an inversely proportional manner by the squared-magnitude of the degradation operator. For instance, frequencies corresponding to degradation-filter magnitudes lower than 1 lead to increase in the effective noise-energy addition and in the allocated distortion. The optimal rate allocation (Fig. 3d) is affected by the signal-to-noise ratio and by the squared-magnitude of the degradation filter (see also Eq. (55)), e.g., components that are attenuated by the degradation operator get less bits in the rate allocation.

D. Conceptual Relation to The Proposed Approach

In general, theoretical studies of rate-distortion problems for the Gaussian case provide to the signal processing practice optimistic beliefs about which design concepts perform well for the real-world non-Gaussian instances of the problems (see the excellent discussion in [25, Sec. 3]). Moreover, theoretical and practical solutions may embody in a different way the same general concepts. Therefore, one should look for connections between theory and practice in the form of high-level analogies.

The optimal solution presented in this section considers the classical framework of rate-distortion theory and a particular, however, important case of Gaussian signal and LSI degradation operator. Our rate-distortion analysis showed that the optimal complexity-regularized restoration consists of the following two main ideas: pseudoinverse filtering of the degraded input, and compression with respect to a squared-error metric that is weighted based on the degradation-filter squared-magnitude (considering the DFT-domain procedure). We will now turn to explain how these two concepts connect to more general themes having different realizations in the practical approach proposed in Section III ¹.

• **Design Concept #1: Apply simple restoration filtering.** The general idea of using an elementary restoration filter is implemented in the Gaussian case as pseudoinverse filtering. Cor-

¹Since the differences between Algorithms 1 and 2 are for a shift-invariance purpose, an issue that we do not concern in this section, we compare our theoretic results only to Algorithm 1.

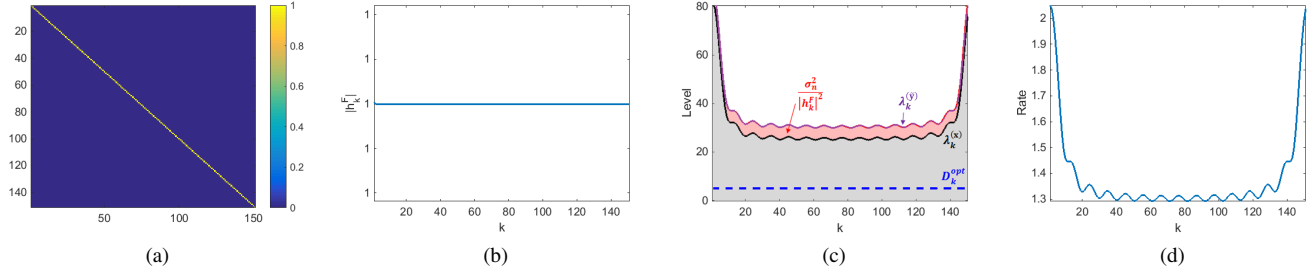


Fig. 2. Demonstrating the theoretic results for a denoising problem with a noise level of $\sigma_n^2 = 5$. (a) The degenerated degradation operator in the signal domain $\mathbf{H} = \mathbf{I}$. (b) DFT-domain magnitude of the degradation filter. (c) Optimal waterfilling solution in DFT domain. (d) Optimal rate allocation in DFT domain.

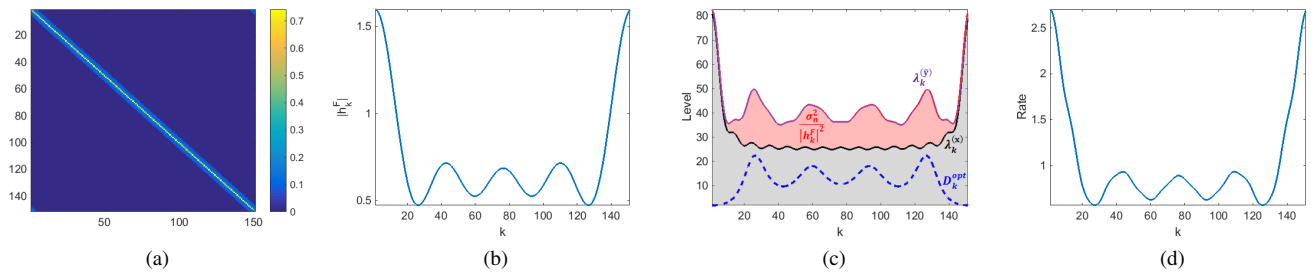


Fig. 3. Demonstrating the theoretic results for a restoration problem with a noise level of $\sigma_n^2 = 5$. (a) The degradation operator in the signal domain \mathbf{H} . (b) DFT-domain magnitude of the degradation filter. (c) Optimal waterfilling solution in DFT domain. (d) Optimal rate allocation in DFT domain.

respondingly, our practical approach relies on a simple filtering mechanism, extending the pseudoinverse filter as explained next. Stage 4 of Algorithm 1 is an ℓ_2 -constrained deconvolution filtering that, using the relation $\mathbf{H}^* (\mathbf{I} - \mathbf{H}\mathbf{H}^*) = \mathbf{0}$, can be rewritten as (see proof in Appendix D)

$$\hat{\mathbf{x}}^{(t)} = \left(\mathbf{H}^* \mathbf{H} + \frac{\beta^{(t)}}{2} \mathbf{I} \right)^{-1} \left(\mathbf{H}^* \mathbf{H} \tilde{\mathbf{y}} + \frac{\beta^{(t)}}{2} \hat{\mathbf{z}}^{(t-1)} \right). \quad (56)$$

As before, $\tilde{\mathbf{y}} = \mathbf{H}^+ \mathbf{y}$, i.e., the pseudoinverse-filtered version of \mathbf{y} . The expression (56) can be interpreted as an initial pseudoinverse filtering of the degraded input, followed by a simple weighted averaging with $\hat{\mathbf{z}}^{(t-1)}$ (the decompressed signal obtained in the last iteration). Evidently, the filtering in (56) is determined by the $\beta^{(t)}$ value, specifically, for $\beta^{(t)} = 0$ the estimate coincides with the pseudoinverse filtering solution and as $\beta^{(t)}$ grows it gets closer to $\hat{\mathbf{z}}^{(t-1)}$.

• **Design Concept #2: Compress by promoting higher quality for signal-components matching to higher h -operator magnitudes.** This principle is realized in the theoretic Gaussian case as weights attached to the squared-errors of DFT-domain components (see Problems 3 and 4). Since the weights, $(|h_0^F|^2, \dots, |h_{N-1}^F|^2)$, are the squared magnitudes of the corresponding degradation-filter coefficients, the compression distortion is spread unevenly being larger where the degradation filter-magnitude is lower. Remarkably, this concept is implemented differently in the proposed procedure (Algorithm 1) where regular compression techniques, optimized for the squared-error distortion measure, are applied on the filtering result of the preceding stage. Let us revisit (56), expressing

stage 4 of Algorithm 1. Assuming \mathbf{H} is a circulant matrix, we can transform (56) into its Fourier domain representation

$$\hat{\mathbf{x}}^{F,(t)} = \left(\mathbf{\Lambda}_H^* \mathbf{\Lambda}_H + \frac{\beta^{(t)}}{2} \mathbf{I} \right)^{-1} \left(\mathbf{\Lambda}_H^* \mathbf{\Lambda}_H \tilde{\mathbf{y}}^F + \frac{\beta^{(t)}}{2} \hat{\mathbf{z}}^{F,(t-1)} \right) \quad (57)$$

where $\hat{\mathbf{x}}^{F,(t)}$ and $\hat{\mathbf{z}}^{F,(t-1)}$ are the Fourier representations of $\hat{\mathbf{x}}^{(t)}$ and $\hat{\mathbf{z}}^{(t-1)}$, respectively. Furthermore, (57) reduces to the componentwise formulation

$$\hat{x}_k^{F,(t)} = \frac{|h_k^F|^2 \tilde{y}_k^F + \frac{\beta^{(t)}}{2} \hat{z}_k^{F,(t-1)}}{|h_k^F|^2 + \frac{\beta^{(t)}}{2}} \quad (58)$$

where $\hat{x}_k^{F,(t)}$ and $\hat{z}_k^{F,(t-1)}$ are the k^{th} Fourier coefficients of $\hat{\mathbf{x}}^{F,(t)}$ and $\hat{\mathbf{z}}^{F,(t-1)}$, respectively. Equation (58) shows that signal elements corresponding to degradation-filter components of weaker energies will be retracted more closely to the decompressed signal obtained in the former iteration (where the compression in general was of a lower quality) – thus, will be also of a relatively lower quality in the compression applied in the next stage of this iteration.

To conclude this section, we showed that the main architectural ideas expressed in theory (for the Gaussian case) appear also in our practical procedure. The iterative nature of our methods (Algorithms 1-2) as well as the desired shift-invariance property provided by Algorithm 2 are outcomes of treating real-world scenarios such as non-Gaussian signals, general linear degradation operators, and computational limitations leading to block-based treatments – these all relate

to practical aspects, hence, do not affect the fundamental treatment given in this section.

V. EXPERIMENTAL RESULTS

In this section we present experimental results for image restoration. Our study cases include deblurring and inpainting using the image-compression profile of the HEVC standard.

We empirically found it sufficient to consider only a part of all the shifts, i.e., a portion of \mathcal{B}^* . The limited amount of shifts is compensated by the HEVC architecture that employs inter-block spatial predictions, thus, improves upon methods relying on independent block treatment. The shifts are defined by the rectangular images having their upper-left corner pixel relatively close to the upper-left corner of the full image, and their bottom-right corner pixel coincides with that of the full image. This extends the mathematical developments in Section III as practical compression handles arbitrarily sized rectangular images.

A. Image Deblurring

Here we consider two deterioration settings taken from [26]. The first setting, denoted in Table I as 'Set. 1', considers a noise variance $\sigma_n^2 = 2$ coupled with a blur operator defined by the two-dimensional point-spread-function (PSF) $h(x_1, x_2) = 1/(1 + x_1^2 + x_2^2)$ for $x_1, x_2 = -7, \dots, 7$, and zero-valued otherwise. The second setting, denoted in Table I as 'Set. 2' (named in [26] as 'Scenario 3'), considers a noise variance $\sigma_n^2 \approx 0.3$ joint with a blur operator defined by the two-dimensional uniform blur PSF of size 9×9 .

Our method results in this subsection are for implementation employing the HEVC still-image compression (in its BPG implementation [27]). In both experimental settings (i.e., 'Set. 1' and 'Set. 2') the quality parameter for the HEVC was decreased by one (starting at 51) in each iteration, and $\beta^{(t)} = (2 \times 10^{-3}) \cdot 1.01^{t-1}$ (where iteration numbers are integers starting at $t = 1$). We run 18 and 33 iterations for experimental settings 1 and 2, respectively. We use here 4 shifts defined by their top-left pixels at the coordinates $\{(1,1), (1,9), (9,1), (9,9)\}$ of the input image. Table I shows a comparison between various deblurring methods tested in the above two settings for four grayscale images². We argue that our method provides relatively good results for the second settings, since its PSNR improvement exceeds few of the other techniques for each of the test images.

B. Image Inpainting

We presented in [5] experimental results for the inpainting problem, in its noisy and noiseless settings. Here we focus on the noiseless inpainting problem, where only pixel erasure occurs without an additive noise. The degradation is represented by a diagonal matrix \mathbf{H} of $N \times N$ size with main diagonal values of zeros and ones, indicating positions of missing and available pixels, respectively. Then, the product $\mathbf{H}\mathbf{x}$ equals to an N -length vector where its k^{th} sample is

²The results in Table I for the methods from [26], [28]–[32] were taken as is from [26].

determined by \mathbf{H} : if $\mathbf{H}[k, k] = 0$ then it is zero, and for $\mathbf{H}[k, k] = 1$ it equals to the corresponding sample of \mathbf{x} . The structure of the pixel erasure operator let us to simplify the optimization in step 4 of Algorithm 2. We note that \mathbf{H} is a square diagonal matrix and, therefore, $\mathbf{H}^T = \mathbf{H}$ and $\mathbf{H}^T\mathbf{y}$ is equivalent to a vector \mathbf{y} with zeroed components according to \mathbf{H} 's structure. Additional useful relations are $\mathbf{H}^T\mathbf{H} = \mathbf{H}$ and that $\mathbf{W} \triangleq \sum_{i \in \mathcal{B}^*} \mathbf{P}_i^T \mathbf{P}_i$ is a diagonal matrix. Consequently, step 4 of Algorithm 2 facilitates a componentwise computation that, together with the fact that there is no noise, is interpreted to form the k^{th} sample of $\hat{\mathbf{x}}^{(t)}$ as

$$\hat{\mathbf{x}}^{(t)}[k] = \begin{cases} \mathbf{y}[k] & , \text{for } \mathbf{H}[k, k] = 1 \\ \frac{\hat{\mathbf{z}}_{sum}^{(t-1)}[k]}{\mathbf{W}[k, k]} & , \text{for } \mathbf{H}[k, k] = 0. \end{cases} \quad (59)$$

We initialize $\hat{\mathbf{z}}_{sum}^{(0)} = \mathbf{H}\mathbf{y} + 128 \cdot (\mathbf{I} - \mathbf{H})$. The rest of the procedure remains as before.

Our implementation here of Algorithm 2 utilizes the HEVC image compression [27]. Running 100 iterations, we start at the highest compression parameter 51 (i.e., the lowest quality) and decrease it by one every three iterations. The used shifts are defined by a 5×5 grid starting at the top-left pixel of the input image and determining the top-left pixels of the shifted images by horizontal and vertical spacings of 5 pixels.

We consider the experimental settings from [33], where 80% of the pixels are missing (see Fig. 6b and 7b). Five competing inpainting methods are considered: cubic interpolation of missing pixels via Delaunay triangulation (using Matlab's 'griddata' function); inpainting using sparse representations of patches of 16×16 pixels based on an overcomplete DCT (ODCT) dictionary (see method description in [34, Ch. 15]); using patch-group transformation [35]; based on patch clustering [36]; and via patch reordering [33]. The PSNR values of images restored using the above methods (taken from [33]) are provided in Table II together with our results. For each of the tested images our method exceeds several competing methods – particularly, for the Lena image we are second only to [36]. Visually, Figures 6c and 7c exhibit the effectiveness of our method in repairing the vast amount of absent pixels.

VI. CONCLUSION

In this paper we explored the topic of complexity-regularized restoration. Two practical methods for restoration using standard compression techniques were introduced, one of them relies on a new shift-invariant complexity regularizer. We presented an insightful theoretical-analysis of complexity-regularized restoration of a cyclo-stationary Gaussian signal from deterioration of a linear shift-invariant operator and additive white Gaussian noise. Experiments for deblurring and inpainting of images using the HEVC technique showed good results.

TABLE I
DEBLURRING: COMPARISON OF PSNR GAINS

| | Cameraman 256x256 | | House 256x256 | | Lena 512x512 | | Barbara 512x512 | |
|---------------|----------------------|--------------|------------------|--------------|-----------------|-------------|--------------------|-------------|
| | Set. 1 | Set. 2 | Set. 1 | Set. 2 | Set. 1 | Set. 2 | Set. 1 | Set. 2 |
| Input PSNR | 22.23 | 20.76 | 25.61 | 24.11 | 27.25 | 25.84 | 23.34 | 22.49 |
| ForWaRD [28] | 6.76 | 7.34 | 7.35 | 9.56 | 6.05 | 6.97 | 3.69 | 4.02 |
| SV-GSM [29] | 7.45 | 7.33 | 8.64 | 9.04 | - | - | 6.85 | 5.07 |
| BM3DDEB [30] | 8.19 | 8.34 | 9.32 | 10.85 | 7.95 | 7.97 | 7.80 | 5.86 |
| TVMM [31] | 7.41 | 8.54 | 7.98 | 10.39 | 6.36 | 7.47 | 3.10 | 3.49 |
| CGMK [32] | 7.80 | 9.15 | 8.31 | 10.75 | 6.76 | 7.86 | 2.45 | 3.55 |
| IDD-BM3D [26] | 8.85 | 10.45 | 9.95 | 12.89 | 7.97 | 8.91 | 7.64 | 6.05 |
| EPLL [7] | 7.17 | 8.78 | 8.27 | 11.76 | 7.39 | 8.55 | 4.28 | 4.29 |
| Proposed | 5.97 | 7.55 | 6.06 | 11.08 | 4.68 | 7.47 | 4.75 | 3.71 |



Fig. 4. The deblurring experiment (settings #2) for the Cameraman image (256 × 256). (a) The underlying image. (b) degraded image (20.77 dB). (c) restored image using HEVC compression (28.32 dB).



Fig. 5. The deblurring experiment (settings #2) for the Barbara image (512 × 512). (a) The underlying image. (b) degraded image (22.49 dB). (c) restored image using HEVC compression (26.20 dB).

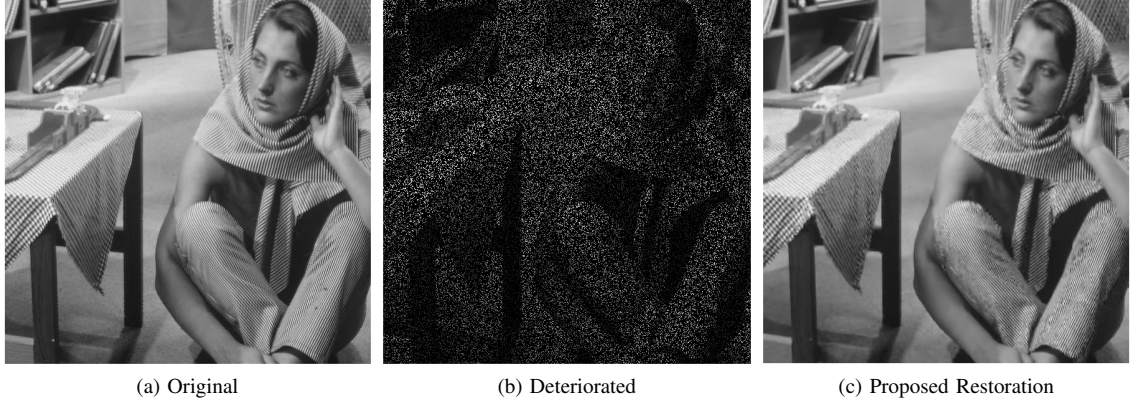


Fig. 6. The inpainting experiment (80% missing pixels) for the Barbara image (512×512). (a) The original image. (b) deteriorated image. (c) restored image using HEVC compression (28.14 dB).

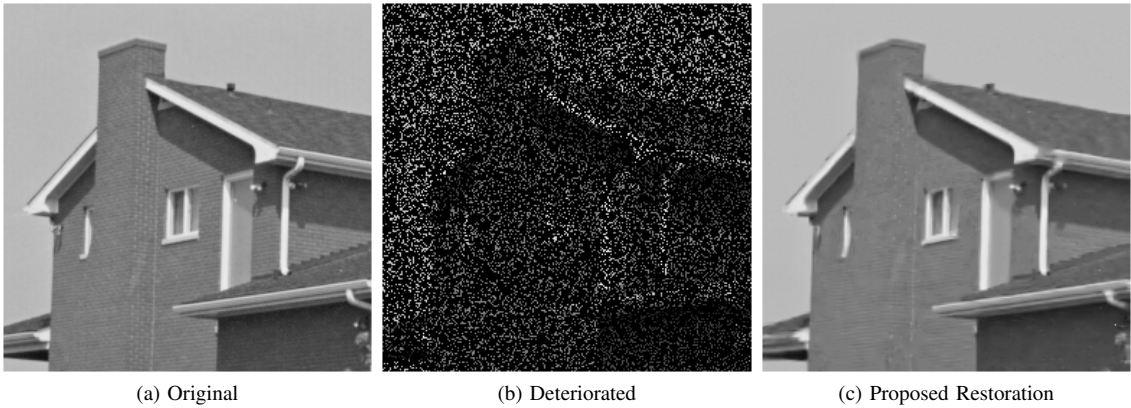


Fig. 7. The inpainting experiment (80% missing pixels) for the House image (256×256). (a) The original image. (b) deteriorated image. (c) restored image using HEVC compression (32.52 dB).

TABLE II
IMAGE INPAINTING FROM 80% MISSING PIXELS
PSNR RESULTS

| Image | Delaunay Triang. | ODCT | Li [35] | Yu et al. [36] | Ram et al. [33] | Proposed |
|-----------------|------------------|-------|---------|----------------|-----------------|----------|
| Lena 512x512 | 30.25 | 29.97 | 31.62 | 32.22 | 31.96 | 32.14 |
| Barbara 512x512 | 22.88 | 27.15 | 25.40 | 30.94 | 29.71 | 28.14 |
| House 256x256 | 29.21 | 29.69 | 32.87 | 33.05 | 32.71 | 32.52 |

$$\begin{aligned}
 & + \mathbf{y}^* (\mathbf{I} - \mathbf{H}\mathbf{H}^+)^* \mathbf{H} (\mathbf{H}^+ \mathbf{y} - \hat{\mathbf{x}}) \\
 & = \|(\mathbf{I} - \mathbf{H}\mathbf{H}^+) \mathbf{y}\|_2^2 + \|\mathbf{H} (\mathbf{H}^+ \mathbf{y} - \hat{\mathbf{x}})\|_2^2
 \end{aligned} \quad (60)$$

where the last equality follows from

$$\mathbf{H}^* (\mathbf{I} - \mathbf{H}\mathbf{H}^+) = \mathbf{0} \quad (61)$$

that can be easily proved, e.g., by using the DFT-based diagonalization of \mathbf{H} and \mathbf{H}^+ .

The first term in (60) can be further developed:

$$\begin{aligned}
 \|(\mathbf{I} - \mathbf{H}\mathbf{H}^+) \mathbf{y}\|_2^2 & = \|(\mathbf{I} - \mathbf{F}^* \mathbf{\Lambda}_H \mathbf{F} \mathbf{F}^* \mathbf{\Lambda}_H^+ \mathbf{F}) \mathbf{y}\|_2^2 \\
 & = \|\mathbf{F}^* (\mathbf{I} - \mathbf{\Lambda}_H \mathbf{\Lambda}_H^+) \mathbf{F} \mathbf{y}\|_2^2 \\
 & = \|(\mathbf{I} - \mathbf{\Lambda}_H \mathbf{\Lambda}_H^+) \mathbf{y}^F\|_2^2 \\
 & = \sum_{k: h_k^F=0} |y_k^F|^2 = \\
 & = \sum_{k: h_k^F=0} |n_k^F|^2
 \end{aligned} \quad (62)$$

where the last equality is implied from the DFT-component relation $y_k^F = h_k^F x_k^F + n_k^F$ that reduces to $y_k^F = n_k^F$ for

APPENDIX

A. Equivalence of Problems 1 and 2

We start by showing the equality between the distortion constraints of Problems 1 and 2. We develop the distortion of Problem 1 as follows:

$$\begin{aligned}
 \|\mathbf{y} - \mathbf{H}\hat{\mathbf{x}}\|_2^2 & = \|(\mathbf{I} - \mathbf{H}\mathbf{H}^+) \mathbf{y} + \mathbf{H}\mathbf{H}^+ \mathbf{y} - \mathbf{H}\hat{\mathbf{x}}\|_2^2 \\
 & = \|(\mathbf{I} - \mathbf{H}\mathbf{H}^+) \mathbf{y} + \mathbf{H} (\mathbf{H}^+ \mathbf{y} - \hat{\mathbf{x}})\|_2^2 \\
 & = \|(\mathbf{I} - \mathbf{H}\mathbf{H}^+) \mathbf{y}\|_2^2 + \|\mathbf{H} (\mathbf{H}^+ \mathbf{y} - \hat{\mathbf{x}})\|_2^2 \\
 & \quad + (\mathbf{H}^+ \mathbf{y} - \hat{\mathbf{x}})^* \mathbf{H}^* (\mathbf{I} - \mathbf{H}\mathbf{H}^+) \mathbf{y}
 \end{aligned}$$

components with $h_k^F = 0$. Consequently,

$$\begin{aligned} E \left\{ \|(\mathbf{I} - \mathbf{H}\mathbf{H}^+)^* \mathbf{y}\|_2^2 \right\} &= E \left\{ \sum_{k:h_k^F=0} |n_k^F|^2 \right\} \\ &= (N - N_H)\sigma_n^2 \end{aligned} \quad (63)$$

where N_H was defined in Section IV-B as the rank of \mathbf{H} . Accordingly, and also using (60), the distortion constraint of Problem 1, i.e.,

$$E \left\{ \|\mathbf{y} - \mathbf{H}\hat{\mathbf{x}}\|_2^2 \right\} = N\sigma_n^2 \quad (64)$$

equals to (recall that $\tilde{\mathbf{y}} = \mathbf{H}^+ \mathbf{y}$)

$$E \left\{ \|\mathbf{H}(\tilde{\mathbf{y}} - \hat{\mathbf{x}})\|_2^2 \right\} = N_H\sigma_n^2, \quad (65)$$

that is, the distortion constraint of Problem 2.

We now turn to prove the equivalence of Problems 1 and 2. Our proof sketch conforms with common arguments in rate-distortion function proofs (see [24]): first, we lower bound the mutual information $I(\mathbf{y}, \hat{\mathbf{x}})$, which is the cost function of Problem 1; then, we provide a statistical construction achieving the lower bound while obeying the distortion constraint.

The proposed lower bound for $I(\mathbf{y}, \hat{\mathbf{x}})$ is established by noting that $\tilde{\mathbf{y}} = \mathbf{H}^+ \mathbf{y}$ and, therefore, the data processing inequality [24] implies here that

$$I(\mathbf{y}, \hat{\mathbf{x}}) \geq I(\tilde{\mathbf{y}}, \hat{\mathbf{x}}), \quad (66)$$

where $I(\tilde{\mathbf{y}}, \hat{\mathbf{x}})$ is the cost function of Problem 2. The relation in (66) is known to be attained with equality when \mathbf{y} and $\hat{\mathbf{x}}$ are independent given $\tilde{\mathbf{y}}$. The next construction shows that this is indeed the case.

We will now show the achievability of the lower bound in (66) by describing a setting corresponding to the conditional PDF $p_{\tilde{\mathbf{y}}|\hat{\mathbf{x}}}(\tilde{y}|\hat{x})$, also known as the (backward) test channel [24], statistically representing $\tilde{\mathbf{y}}$ as an outcome of $\hat{\mathbf{x}}$. We consider the construction

$$\hat{\mathbf{x}} \sim \mathcal{N}(\mathbf{0}, \mathbf{H}^+ \mathbf{R}_y \mathbf{H}^{+*} - \sigma_n^2 \mathbf{H}^+ \mathbf{H}^{+*}) \quad (67)$$

$$\mathbf{z} \sim \mathcal{N}(\mathbf{0}, \sigma_n^2 \mathbf{H}^+ \mathbf{H}^{+*}) \quad (68)$$

where $\hat{\mathbf{x}}$ and \mathbf{z} are independent. Consequently, we define

$$\tilde{\mathbf{y}} = \hat{\mathbf{x}} + \mathbf{z}, \quad (69)$$

implying $\tilde{\mathbf{y}} \sim \mathcal{N}(\mathbf{0}, \mathbf{H}^+ \mathbf{R}_y \mathbf{H}^{+*})$ that, indeed, conforms with $\tilde{\mathbf{y}} = \mathbf{H}^+ \mathbf{y}$ where $\mathbf{y} \sim \mathcal{N}(\mathbf{0}, \mathbf{R}_y)$. Moreover, the construction (67)-(69) yields

$$\begin{aligned} E \left\{ \|\mathbf{H}(\tilde{\mathbf{y}} - \hat{\mathbf{x}})\|_2^2 \right\} &= E \left\{ \|\mathbf{H}\mathbf{z}\|_2^2 \right\} \\ &= E \left\{ \mathbf{z}^* \mathbf{H}^* \mathbf{H}\mathbf{z} \right\} \\ &= E \left\{ \text{Trace} \left\{ \mathbf{z}^* \mathbf{H}^* \mathbf{H}\mathbf{z} \right\} \right\} \\ &= E \left\{ \text{Trace} \left\{ \mathbf{H}\mathbf{z}\mathbf{z}^* \mathbf{H}^* \right\} \right\} \\ &= \text{Trace} \left\{ \mathbf{H}\mathbf{R}_z \mathbf{H}^* \right\} \\ &= \sigma_n^2 \cdot \text{Trace} \left\{ \mathbf{H}\mathbf{H}^+ \mathbf{H}^{+*} \mathbf{H}^* \right\} \\ &= \sigma_n^2 N_H \end{aligned} \quad (70)$$

thus, satisfying the distortion constraint (65). Our next task is to prove that \mathbf{y} and $\hat{\mathbf{x}}$ are independent given $\tilde{\mathbf{y}}$. The simple relation $\mathbf{y} = \mathbf{H}\mathbf{H}^+ \mathbf{y} + (\mathbf{I} - \mathbf{H}\mathbf{H}^+)^* \mathbf{y}$ lets us considering \mathbf{y} to emerge from $\tilde{\mathbf{y}}$ via

$$\mathbf{y} = \mathbf{H}\tilde{\mathbf{y}} + \mathbf{w} \quad (71)$$

where $\mathbf{w} = (\mathbf{I} - \mathbf{H}\mathbf{H}^+)^* \mathbf{y}$. First, one can verify that the distortion constraint of Problem 1 is satisfied. Second, the random vectors $\mathbf{H}\tilde{\mathbf{y}}$ and \mathbf{w} are uncorrelated due to

$$\begin{aligned} E \left\{ \mathbf{w}^* \mathbf{H}\tilde{\mathbf{y}} \right\} &= E \left\{ \mathbf{y}^* (\mathbf{I} - \mathbf{H}\mathbf{H}^+)^* \mathbf{H}\tilde{\mathbf{y}} \right\} \\ &= E \left\{ \mathbf{y}^* \mathbf{0} \tilde{\mathbf{y}} \right\} \\ &= 0. \end{aligned} \quad (72)$$

Since $\mathbf{H}\tilde{\mathbf{y}}$ and \mathbf{w} are Gaussian, they are also independent. Additionally, $\tilde{\mathbf{y}} = \mathbf{H}^+ \mathbf{y}$ implies that $\tilde{\mathbf{y}}$ and \mathbf{w} are also independent Gaussian vectors. Then, (69) and (71) means that $\hat{\mathbf{x}} \rightarrow \tilde{\mathbf{y}} \rightarrow \mathbf{y}$ is a Markov chain and, therefore, \mathbf{y} and $\hat{\mathbf{x}}$ are independent given $\tilde{\mathbf{y}}$. This evident construction turns (66) into

$$I(\mathbf{y}, \hat{\mathbf{x}}) = I(\tilde{\mathbf{y}}, \hat{\mathbf{x}}) \quad (73)$$

that completes proving the equivalence of Problems 1 and 2.

B. Equivalence of Problems 2 and 3

The rate-distortion function for a Gaussian source with memory (i.e., correlated components) is usually derived in the Principle Component Analysis (PCA) domain where the components are independent Gaussian variables (see, e.g., [37]). In our case, where the signal is cyclo-stationary, the PCA is obtained using the DFT matrix. As in the usual case,

$$I(\tilde{\mathbf{y}}, \hat{\mathbf{x}}) = I(\tilde{\mathbf{y}}^F, \hat{\mathbf{x}}^F) \quad (74)$$

$$= \sum_{k=0}^{N-1} I(\tilde{y}_k^F, \hat{x}_k^F) \quad (75)$$

where (74) emerges from the reversibility of the transformation, and (75) is due to the independence of the $\{\tilde{y}_k^F\}_{k=0}^{N-1}$ components [24].

The main difference from the well-known rate-distortion analysis is that here, in Problem 2, the distortion constraint is not a regular squared error – but a weighted one, that will be developed next. Since DFT is a unitary transformation, its energy preservation property yields

$$\begin{aligned} E \left\{ \|\mathbf{H}(\tilde{\mathbf{y}} - \hat{\mathbf{x}})\|_2^2 \right\} &= E \left\{ \|\mathbf{H}\mathbf{z}\|_2^2 \right\} \\ &= \sum_{k=0}^{N-1} |h_k^F|^2 E \left\{ |\tilde{y}_k^F - \hat{x}_k^F|^2 \right\} \end{aligned} \quad (76)$$

where the last equality is due to the diagonal structure of \mathbf{H} . Hence, we got that the two expected-distortion expressions in Problems 2 and 3 are equal.

C. Solution of Problem 4

For start, the transition between Problem 3 and Problem 4 is analogous to the familiar case of jointly coding a set of independent Gaussian variables [24]. Accordingly, and also due to lack of space, we do not elaborate here on this problem-equivalence proof.

Problem 4 is compelling as it is a distortion-allocation optimization, where the distortion levels $\{D_k\}_{k=0}^{N-1}$ are allocated under the joint distortion constraint. We address Problem 4 via its Lagrangian form (temporarily ignoring the constraints of non-negative distortions)

$$\min_{D_0, \dots, D_{N-1}} \sum_{k=0}^{N-1} \left[\frac{1}{2} \log \left(\frac{\lambda^{(\bar{y}_k)}}{D_k} \right) \right]_+ + \mu \sum_{k=0}^{N-1} |h_k^F|^2 D_k \quad (77)$$

where $\mu \geq 0$ is the Lagrange multiplier. Recalling that some components may correspond to $h_k^F = 0$ and, by (48), also $\lambda_k^{(\bar{y})} = 0$ – meaning they are deterministic variables. These deterministic components do not need to be coded (i.e., $R_k = 0$) while still attaining $D_k = 0$. Accordingly, the Lagrangian optimization (77) is updated into

$$\min_{\{D_k\}_{k:h_k^F \neq 0}} \sum_{k:h_k^F \neq 0} \frac{1}{2} \log \left(\frac{\lambda_k^{(\bar{x})} + \frac{\sigma_n^2}{|h_k^F|^2}}{D_k} \right) + \mu \sum_{k:h_k^F \neq 0} |h_k^F|^2 D_k \quad (78)$$

where we used the expression from (48), and assumed that the distortions are small enough such that the operator $[\cdot]_+$ can be omitted (a correct assumption as will be later shown). Now, the optimal D_k value can be determined by equating the respective derivative of the Lagrangian cost to zero, leading to allocated distortion (still as a function of μ)

$$D_k^{opt} = \frac{1}{2 \ln(2) \mu |h_k^F|^2} \quad \text{for } k : h_k^F \neq 0 \quad (79)$$

and by setting the μ satisfying the total distortion constraint from Problem 4 we get

$$D_k^{opt} = \frac{\sigma_n^2}{|h_k^F|^2} \quad \text{for } k : h_k^F \neq 0. \quad (80)$$

Expressing a nonuniform distortion-allocation (for components with nonzero h_k^F), being inversely proportional to the weights $\{|h_k^F|^2\}_{k=0}^{N-1}$. One should note that the assumption on small-enough distortions is satisfied as $D_k^{opt} \leq \lambda_k^{(\bar{y})}$ for any k obeying $h_k^F \neq 0$, and that all the distortions are non-negative as required. The optimal distortions established here (for k where $h_k^F \neq 0$) are set in the rate formula (51), providing the optimal rate allocation

$$R_k^{opt} = \begin{cases} \frac{1}{2} \log \left(|h_k^F|^2 \frac{\lambda_k^{(\bar{x})}}{\sigma_n^2} + 1 \right) & \text{for } h_k^F \neq 0 \\ 0 & \text{for } h_k^F = 0. \end{cases} \quad (81)$$

D. Equivalent Form of Stage 4 of Algorithm 1

Stage 4 of Algorithm 1 is considered here with the conjugate-transpose operator, $*$, extending the regular transpose:

$$\hat{x}^{(t)} = \left(\mathbf{H}^* \mathbf{H} + \frac{\beta^{(t)}}{2} \mathbf{I} \right)^{-1} \left(\mathbf{H}^* \mathbf{y} + \frac{\beta^{(t)}}{2} \hat{\mathbf{z}}^{(t-1)} \right). \quad (82)$$

We note that

$$\begin{aligned} \mathbf{H}^* \mathbf{y} &= \mathbf{H}^* (\mathbf{H} \mathbf{H}^* \mathbf{y} + (\mathbf{I} - \mathbf{H} \mathbf{H}^*) \mathbf{y}) \\ &= \mathbf{H}^* \mathbf{H} \tilde{\mathbf{y}} + \mathbf{H}^* (\mathbf{I} - \mathbf{H} \mathbf{H}^*) \mathbf{y} \\ &= \mathbf{H}^* \mathbf{H} \tilde{\mathbf{y}} \end{aligned} \quad (83)$$

where the last equality results from the relation $\mathbf{H}^* (\mathbf{I} - \mathbf{H} \mathbf{H}^*) = \mathbf{0}$. Consequently, (82) becomes

$$\hat{x}^{(t)} = \left(\mathbf{H}^* \mathbf{H} + \frac{\beta^{(t)}}{2} \mathbf{I} \right)^{-1} \left(\mathbf{H}^* \mathbf{H} \tilde{\mathbf{y}} + \frac{\beta^{(t)}}{2} \hat{\mathbf{z}}^{(t-1)} \right), \quad (84)$$

which is the form presented in (56).

REFERENCES

- [1] B. K. Natarajan, “Filtering random noise from deterministic signals via data compression,” *IEEE Trans. Signal Process.*, vol. 43, no. 11, pp. 2595–2605, 1995.
- [2] J. Rissanen, “MDL denoising,” *IEEE Trans. Inf. Theory*, vol. 46, no. 7, pp. 2537–2543, 2000.
- [3] J. Liu and P. Moulin, “Complexity-regularized image denoising,” *IEEE Trans. Image Process.*, vol. 10, no. 6, pp. 841–851, 2001.
- [4] P. Moulin and J. Liu, “Statistical imaging and complexity regularization,” *IEEE Trans. Inf. Theory*, vol. 46, no. 5, pp. 1762–1777, 2000.
- [5] Y. Dar, A. M. Bruckstein, and M. Elad, “Image restoration via successive compression,” in *Picture Coding Symposium (PCS)*, 2016, pp. 1–5.
- [6] D. Geman and C. Yang, “Nonlinear image recovery with half-quadratic regularization,” *IEEE Trans. Image Process.*, vol. 4, no. 7, pp. 932–946, 1995.
- [7] D. Zoran and Y. Weiss, “From learning models of natural image patches to whole image restoration,” in *IEEE International Conference on Computer Vision (ICCV)*, 2011, pp. 479–486.
- [8] S. V. Venkatakrishnan, C. A. Bouman, and B. Wohlberg, “Plug-and-play priors for model based reconstruction,” in *IEEE GlobalSIP*, 2013.
- [9] Y. Romano, M. Elad, and P. Milanfar, “The little engine that could: Regularization by denoising (red),” *SIAM Journal on Imaging Sciences*, vol. 10, no. 4, pp. 1804–1844, 2017.
- [10] Y. Dar, A. M. Bruckstein, M. Elad, and R. Giryes, “Postprocessing of compressed images via sequential denoising,” *IEEE Trans. Image Process.*, vol. 25, no. 7, pp. 3044–3058, 2016.
- [11] ———, “Reducing artifacts of intra-frame video coding via sequential denoising,” in *IEEE International Conference on the Science of Electrical Engineering (ICSEE)*, 2016, pp. 1–5.
- [12] A. Rond, R. Giryes, and M. Elad, “Poisson inverse problems by the plug-and-play scheme,” *Journal of Visual Communication and Image Representation*, vol. 41, pp. 96–108, 2016.
- [13] R. R. Coifman and D. L. Donoho, “Translation-invariant de-noising,” in *Wavelets and Statistics*. Springer, 1995, pp. 125–150.
- [14] A. Nosratinia, “Enhancement of JPEG-compressed images by re-application of JPEG,” *J. VLSI Signal Process. Syst. for Signal, Image and Video Technol.*, vol. 27, no. 1-2, pp. 69–79, 2001.
- [15] ———, “Postprocessing of JPEG-2000 images to remove compression artifacts,” *IEEE Signal Process. Lett.*, vol. 10, no. 10, 2003.
- [16] S. Beygi, S. Jalali, A. Maleki, and U. Mitra, “Compressed sensing of compressible signals,” in *IEEE International Symposium on Information Theory (ISIT)*, 2017, pp. 2158–2162.
- [17] ———, “An efficient algorithm for compression-based compressed sensing,” *arXiv preprint arXiv:1704.01992*, 2017.
- [18] G. J. Sullivan, J. Ohm, W.-J. Han, and T. Wiegand, “Overview of the high efficiency video coding (HEVC) standard,” *IEEE Trans. on Circuits Syst. Video Technol.*, vol. 22, no. 12, pp. 1649–1668, 2012.

- [19] I. Galić, J. Weickert, M. Welk, A. Bruhn, A. Belyaev, and H.-P. Seidel, “Image compression with anisotropic diffusion,” *Journal of Mathematical Imaging and Vision*, vol. 31, no. 2, pp. 255–269, 2008.
- [20] C. Schmalz, J. Weickert, and A. Bruhn, “Beating the quality of JPEG 2000 with anisotropic diffusion.” in *DAGM-Symposium*. Springer, 2009, pp. 452–461.
- [21] S. Andris, P. Peter, and J. Weickert, “A proof-of-concept framework for PDE-based video compression,” in *Picture Coding Symposium (PCS)*, 2016, pp. 1–5.
- [22] Y. Shoham and A. Gersho, “Efficient bit allocation for an arbitrary set of quantizers,” *IEEE Trans. Acoust., Speech, Signal Process.*, vol. 36, no. 9, pp. 1445–1453, 1988.
- [23] A. Ortega and K. Ramchandran, “Rate-distortion methods for image and video compression,” *IEEE Signal Process. Mag.*, vol. 15, no. 6, pp. 23–50, 1998.
- [24] T. M. Cover and J. A. Thomas, *Elements of information theory*. John Wiley & Sons, 2012.
- [25] D. L. Donoho, M. Vetterli, R. A. DeVore, and I. Daubechies, “Data compression and harmonic analysis,” *IEEE Trans. Inf. Theory*, vol. 44, no. 6, pp. 2435–2476, 1998.
- [26] A. Danielyan, V. Katkovnik, and K. Egiazarian, “BM3D frames and variational image deblurring,” *IEEE Trans. Image Process.*, vol. 21, no. 4, pp. 1715–1728, 2012.
- [27] F. Bellard, “BPG 0.9.6.” [Online]. Available: <http://bellard.org/bpg>
- [28] R. Neelamani, H. Choi, and R. Baraniuk, “ForWaRD: Fourier-wavelet regularized deconvolution for ill-conditioned systems,” *IEEE Trans. Signal Process.*, vol. 52, no. 2, pp. 418–433, 2004.
- [29] J. A. Guerrero-Colón, L. Mancera, and J. Portilla, “Image restoration using space-variant gaussian scale mixtures in overcomplete pyramids,” *IEEE Trans. Image Process.*, vol. 17, no. 1, pp. 27–41, 2008.
- [30] K. Dabov, A. Foi, V. Katkovnik, and K. O. Egiazarian, “Image restoration by sparse 3D transform-domain collaborative filtering.” in *Image Processing: Algorithms and Systems*, 2008, p. 681207.
- [31] J. P. Oliveira, J. M. Bioucas-Dias, and M. A. Figueiredo, “Adaptive total variation image deblurring: a majorization–minimization approach,” *Signal Processing*, vol. 89, no. 9, pp. 1683–1693, 2009.
- [32] G. Chantas, N. P. Galatsanos, R. Molina, and A. K. Katsaggelos, “Variational bayesian image restoration with a product of spatially weighted total variation image priors,” *IEEE Trans. Image Process.*, vol. 19, no. 2, pp. 351–362, 2010.
- [33] I. Ram, M. Elad, and I. Cohen, “Image processing using smooth ordering of its patches,” *IEEE Trans. Image Process.*, vol. 22, no. 7, pp. 2764–2774, 2013.
- [34] M. Elad, *Sparse and Redundant Representations: From Theory to Applications in Signal and Image Processing*. Springer, 2010.
- [35] X. Li, “Patch-based image interpolation: algorithms and applications.” in *Int. Workshop on Local and Non-Local Approx. in Image Process.*, 2008.
- [36] G. Yu, G. Sapiro, and S. Mallat, “Solving inverse problems with piecewise linear estimators: From Gaussian mixture models to structured sparsity,” *IEEE Trans. Image Process.*, vol. 21, no. 5, pp. 2481–2499, 2012.
- [37] T. Berger, *Rate distortion theory: A mathematical basis for data compression*. Prentice-Hall, 1971.